I&EC research
Industrial & Engineering Chemistry Research

Article

pubs.acs.org/IECR

3D Numerical Simulation of a Large Scale MTO Fluidized Bed Reactor

Yinfeng Zhao, Hua Li, Mao Ye,* and Zhongmin Liu

Dalian National Laboratory for Clean Energy, National Engineering Laboratory for MTO, Dalian Institute of Chemical Physics, Chinese Academy of Sciences, 457 Zhongshan Road, Dalian 116023, China

ABSTRACT: The methanol to olefins (MTO) process has been successfully commercialized in China and will potentially become an important route for light olefins production. In this work, a modeling approach is presented for MTO fluidized bed reactor design and operation optimization. The two-fluid model (TFM) where the solid phase shear viscosity and solid phase pressure are derived from kinetic theory of granular flow has been used to model the solid−gas two-phase flows. The interphase drag force is calculated by either the traditional Gidaspow model or a recently developed EMMS-bubble model. The simulation study has been performed for a fluidized bed reactor in a 16 kt/a DMTO unit. It has been shown that the Gidaspow model cannot predict a stable dense bed, while the EMMS-bubbling model could simulate the solid fraction distribution in the reactor reasonable well. A reaction model based on the simple MTO reaction kinetics has been implemented to test the effectiveness of the model approach. The simulation results show that the methanol is converted rapidly just above the gas inlet. The selectivity of ethylene and propylene however are underpredicted, while the selectivity of CO_2 and other products are overestimated. It is suggested that a further extension of the EMMS model to a turbulent fluidized bed is important in order to get more quantitative results. Also the MTO reaction kinetics for a commercial DMTO catalyst, in which the coke formation kinetics should be included, is highly desired.

1. INTRODUCTION

Light olefins such as ethylene and propylene are traditionally produced by petrochemical routes including naphtha thermal cracking and fluid catalytic cracking (FCC). However, the continuous rising of oil prices in the market in past decades stimulates the desire for novel technology to make ethylene and propylene from alternative resources. The methanol to olefins (MTO) process has attracted considerable attention in recent years because methanol can be readily obtained from coal or natural gas.[1−3] The Dalian Institute of Chemical Physics (DICP), Chinese Academy of Sciences, is among the pioneers of MTO process development, which started to study the conversion of methanol to light olefins using the SAPO-34 catalyst from the later 1980s.[4] The first industrial unit based on DICP MTO (DMTO) technology (1800 kt/a methanol feedstock) had been successfully commissioned in Shenhua's Baotou plant in North China in August 2010. Recently a second DMTO unit (also 1800 kt/a methanol feedstock) has been started in Heyuan's Ningbo plant in East China in February 2013. Meantime, several other industrial DMTO units are under construction in China. Potentially, DMTO will become China's most important route for light olefin production in the future. In commercial DMTO units, the methanol is almost completely converted in a fluidized bed reactor operating in the turbulent fluidization regime with a selectivity of ethylene and propylene of about 80 wt %. The spent catalyst is transported to a bubbling fluidized bed regenerator to restore the activity. The regenerated catalyst is then fed back to the reactor to maintain the high efficiency of methanol conversion. In terms of reactor−regenerator configuration, the DMTO process is similar to the traditional FCC process. However, the DMTO process has many unique features. For example, a turbulent fluidized bed reactor is favored for methanol conversion, while a riser reactor is often used in a modern FCC unit.

Despite the many efforts that have been devoted to catalyst synthesis and reaction kinetics for the MTO process,[3−10] there are few papers in the open literature in which the detailed study of gas−solid two-phase flows in a MTO reactor is reported. The understanding of the hydrodynamics in the MTO fluidized bed is critical for reactor scaling up and design optimization. To this end, a comprehensive study on the gas−solid two-phase flow in a DMTO fluidized bed reactor is initialized in DICP, which includes cold flow experiments and modeling simulations. A cold flow DMTO reactor−regenerator experimental facility is being constructed now in Dalian. Meanwhile, a 3D modeling approach for a DMTO fluidized bed reactor is also under development. This modeling approach is expected to play an important part in improving the reactor design (reactor type, layout, etc.) and optimizing the large scale DMTO demonstration unit (16kt/a methanol feed) operation (temperature, pressure, gas velocity, catalyst circulation rate, etc.).

In general, there are two different approaches widely used for the CFD simulation of gas−solid flows, namely, the Lagrangian and the Eulerian approach. In the Lagrangian approach, particles are treated individually, and their positions are updated at each time step. One of the most often used Lagrangian methods is the discrete element model (DEM) or discrete particle model (DPM).[11−15] In DPM, the track of each particle is computed by solving the Newtonian equations, and

Special Issue: Multiscale Structures and Systems in Process Engineering

Received: December 15, 2012
Revised: June 7, 2013
Accepted: June 7, 2013
Published: June 7, 2013

dx.doi.org/10.1021/ie303467k | *Ind. Eng. Chem. Res.* 2013, 52, 11354−11364

particle−particle collisions are predicted via either the soft-sphere[11,13,15] or hard-sphere method[12]. The influence of gas flow on the particle tracks and verse vice is taken into account by coupling the DPM with a traditional CFD model. The computing time and memory required for a DPM simulation of an industrial scale reactor, however, exceed the computational capacity of computer system at the moment. The Eulerian approach is commonly used for the simulation of large scale fluidized bed reactors. In the Eulerian approach, such as two-fluid model (TFM), the gas and granular phases are treated as fully interpenetrating continua, and the locally averaged Navier−Stokes equations are used for describing the interacting mediums.[16−21] In the TFM, the size and density of solid particles within the solid phase are normally considered to be homogeneous. Because the solid phase is treated as a single phase, which leads to a significant reduction of the number of equations to be solved, the TFM can be used to simulate a relatively large fluidized bed reactor. However, in the TFM, constitutive correlations are required to close the governing equations for both the gas and solid phases, especially the closure laws for the stress−strain relationship of gas and solids, and the momentum transfer between the two phases.[16−24]

In a fluidized bed reactor, gravity and drag are the two dominant forces for the majority of flows.[19] Several drag correlations have been proposed so far to account for the momentum transfer between particles and gas,[22,23,25−30] but the bed expansion of fluidized beds of Geldart A particles has been significantly overestimated by TFM because of the over prediction of the drag force by the traditional drag laws.[31,32] The scaling factor method has been used to simulate the hydrodynamics of fluidized beds of Geldart A particles.[31,32] The bed expansion can be well predicted with an artificially defined scaling factor, but it is still an ad hoc modification. The reason why the traditional drag correlations fail to predict the bed expansion of Geldart A particles is still not completely understood. It has been argued that the heterogeneity induced by the subgrid structure of solid−gas two-phase flows might be the mechanism of such a drag force reduction.[33−40] Traditional drag correlations for solid−gas two-phase systems, which are essentially derived from the experimental data on fixed beds[25] or homogeneous expansion of fluidized beds,[26] exclude the important information of subgrid structures. Recent work by Wang et al.[33−35] directly shows that the lack of scale resolution will probably lead to the failure of the prediction of the fluidization behavior of Geldart A particles in a bubbling fluidized bed, but for an industrial scale fluidized bed reactor, a sufficiently fine grid resolution means unrealistic computational time. In the energy minimization multi-scale (EMMS) model first proposed by Li and Kwark[37] and later extended by the researcher in the same group,[38−40] the influence of subgrid particle clusters on the drag force acting on particles in a control volume has been taken into account. The EMMS model has been successfully applied to the simulations of large scale fluidized bed reactor[41] and fluidized bed boilers[42,43] in recent years and is considered as one of the most promising ways to address the drag forces in the simulation of a large scale gas-fluidized bed. In this work, both the traditional Gidaspow drag force model and the EMMS model are incorporated into the two-fluid model to calculate the interphase drag force. The solid phase shear viscosity and solid phase pressure have been derived from kinetic theory of granular flow.[22,44]

In order to study the reactor performance, a reaction model based on the simple MTO kinetics has been implemented in the 3D modeling approach. In the reaction model, the transport equations of the main components are formulated as 3D diffusion−convection equations. From the reactor engineering point of view, a simple 1D reaction model, which can reduce significantly computational time, is normally sufficient for reactor selection, but the optimal selectivity of ethylene and propylene in MTO reaction is strongly dependent on the coke on the catalyst. Catalysts with a certain distribution of coke will improve the selectivity of the low olefins. The distribution of coke on the catalyst is largely affected by the layout of the catalyst inlet and outlet and gas components distribution in the reactor. Therefore, a simple 1D reaction model may not be possible to give the sufficient information in this regard. Furthermore, for the fluidized bed reactor in the 16 kt/a DMTO demonstration unit, the concentration of main gas components will also have significant gradient in the radial direction. In this work, the 3D diffusion−convection equations are adopted to account for the spatial distribution of the gas components in the reactor. The MTO reaction kinetics is following Najafabadi et al.[45]

It should be argued that, however, building a 3D modeling approach for a larger scale DMTO reactor is not a short-term task because it is dependent upon the understanding of the interaction between the DMTO catalyst and reactant gas, reaction mechanism, and reaction network and kinetics. The work reported in this paper is the first step for such a modeling approach. In the following, we will first introduce the 3D modeling approach. Some preliminary simulation results of the 16 kt/a DMTO demonstration fluidized bed reactor are then presented. We also discuss the further work required to improve the 3D modeling approach for DMTO process.

2. MODELING

2.1. Governing Equations. The continuity equations for the gas and solid phase are given as the following

$$\frac{\partial}{\partial t}(\varepsilon_g\rho_g) + \nabla \times (\varepsilon_g\rho_g v_g) = 0 \tag{1}$$

$$\frac{\partial}{\partial t}(\varepsilon_s\rho_s) + \nabla \times (\varepsilon_s\rho_s v_s) = 0 \tag{2}$$

where ε_k, ρ_k, and v_k represent the volume fraction, density, and velocity of phase k (k = s, g), respectively. The momentum conservation equations for gas and solid phases are given as following

$$\frac{\partial}{\partial t}(\varepsilon_g\rho_g v_g) + \nabla \times (\varepsilon_g\rho_g v_g v_g) = -\varepsilon_g\nabla p + \nabla \times \tau_g + \varepsilon_g\rho_g g + \beta(v_s - v_g) \tag{3}$$

$$\frac{\partial}{\partial t}(\varepsilon_s\rho_s v_s) + \nabla \times (\varepsilon_s\rho_s v_s v_s) = -\varepsilon_s\nabla p - \nabla p_s + \nabla \times \tau_s + \varepsilon_s\rho_s g + \beta(v_g - v_s) \tag{4}$$

In these equations, β is the interphase momentum exchange coefficient. The parameters τ_g and τ_s represent the stress tensors for gas and solid phase, which are defined respectively as

$$\tau_g = -\left[\mu_g((\nabla v_g) + (\nabla v_g)^T) + \left(\lambda_g - \frac{2}{3}\mu_g\right)(\nabla \times v_g)I\right] \tag{5}$$

dx.doi.org/10.1021/ie303467k | Ind. Eng. Chem. Res. 2013, 52, 11354−11364

$$\tau_s = -\left[\mu_s((\nabla v_s) + (\nabla v_s)^T) + \left(\lambda_s - \frac{2}{3}\mu_s\right)(\nabla \times v_s)I\right] \quad (6)$$

2.2. Kinetic Theory of Granular Flow. The solid phase stress is calculated by the kinetic theory of granular flow (KTGF) originally developed by Lun et al.[44] The correlation by Syamlal, Rogers, and O'Brien[46] is used to derive the conductivity of granular energy k_Θ

$$k_\Theta = \frac{15 d_s \rho_s \varepsilon_s \sqrt{\pi\Theta}}{4(41 - 33\eta)}\left[1 + \frac{12}{5}\eta^2(4\eta - 3)\varepsilon_s g_0 + \frac{16}{15\pi}(41 - 33\eta)\eta\varepsilon_s g_0\right] \quad (7)$$

where

$$\eta = \frac{1}{2}(1 + e) \quad (8)$$

The granular temperature Θ is given as

$$\Theta = \frac{1}{3}\langle v'_s\rangle^2 \quad (9)$$

In the above equation, $\langle v'_s\rangle$ represents the ensemble averaged of the random fluctuating velocity of the solid particles. The variation of Θ in time and space is governed by a separate conservation equation, i.e., the so-called granular temperature equation

$$\frac{3}{2}\left[\frac{\partial(\varepsilon_s\rho_s\Theta_s)}{\partial t} + \nabla \times (\varepsilon_s\rho_s\Theta_s v_s)\right] = -(p_s I + \varepsilon_s\tau_s)\colon \nabla v_s + \nabla \times (\varepsilon_s k_{\Theta_s}\nabla\Theta_s) - 3\beta\Theta_s - \gamma_s \quad (10)$$

The solid phase pressure p_s is calculated according to Lun et al.[44]

$$p_s = \varepsilon_s\rho_s\Theta_s[1 + 2(1 + e)\varepsilon_s g_0] \quad (11)$$

Solid phase shear viscosity can be expressed as the summation of the three contributing components

$$\mu_s = \mu_{s.col} + \mu_{s.kin.} + \mu_{s.fr} \quad (12)$$

The term $\mu_{s.col}$ represents the collisional contribution to the shear resistance, and it is defined as follows

$$\mu_{s.col.} = \frac{4}{5}\varepsilon_s\rho_s d_p g_0(1 + e)\sqrt{\frac{\Theta_s}{\pi}} \quad (13)$$

The correlation of kinetic term of the shear viscosity $\mu_{s.kin}$ introduced by Gidaspow[22] is used throughout this work

$$\mu_{s.kin} = \frac{10\rho_s d_p\sqrt{\Theta_s\pi}}{96\varepsilon_s(1 + e)g_0}\left[1 + \frac{4}{5}(1 + e)\varepsilon_s g_0\right]^2 \quad (14)$$

The last term $\mu_{s.fr}$ accounts for the real mechanical friction between the solid particles. This frictional contribution is correlated using the Schaeffer formulation below

$$\mu_{s.fr} = \frac{p_s \sin\theta}{2\sqrt{I_{2D}}} \quad (15)$$

Solid phase bulk viscosity λs formulates the resistance of solid particles to compression and expansion. The following equation given by Lun et al.[44] is used in this work

$$\lambda s = \frac{4}{3}\varepsilon_s\rho_s d_p g_0(1 + e)\sqrt{\frac{\Theta_s}{\pi}} \quad (16)$$

2.3. Drag Model. *2.3.1. Gidaspow Model.* In the momentum transport equations of the individual phase, eqs 3 and 4, the drag force is represented by the term $\beta(v_s - v_g)$, the product of the interphase momentum exchange coefficient and the slip velocity. The correlation as given by Gidaspow has been widely used. The correlation by Gidaspow is a combination of the works of Ergun[25] and Wen and Yu.[26] The Ergun equation is used for dense phase, whereas the formulation by Wen and Yu is used for dilute phase

$$\beta = 150\frac{(1 - \varepsilon_g)^2}{\varepsilon_g}\frac{\mu_g}{(\phi_s d_p)^2} + 1.75(1 - \varepsilon_g)\frac{\rho_g}{(\phi_s d_p)}|v_g - v_s|, \text{ for } \varepsilon_g < 0.8 \quad (17a)$$

$$\beta = \frac{3}{4}C_d\frac{\varepsilon_g(1 - \varepsilon_g)}{(\phi_s d_p)}\rho_g|v_g - v_s|f(\varepsilon_g), \text{ for } \varepsilon_g > 0.8 \quad (17b)$$

where the gas volume fraction ε_g should satisfy

$$f(\varepsilon_g) = \varepsilon_g^{-2.65} \quad (18)$$

and the drag coefficient

$$C_d = \begin{cases} \frac{24}{Re_p}[1 + 0.15(Re_p)^{0.687}], & Re_p < 1000 \\ 0.44, & Re_p > 1000 \end{cases} \quad (19)$$

Note that the particle Reynolds number is defined as

$$Re_p = \frac{\varepsilon_g\rho_g|v_g - v_s|d_p}{\mu_g} \quad (20)$$

In the course of simulations of large scale fluidized bed, the grid size used is normally larger than the size of subgrid structures such as particle clusters or fine bubbles. In order to take these subgrid structures into consideration, a drag force model that accounts for the flow heterogeneity at the grid scale is strongly required. The Ergun equation used in the Gidaspow model was derived from the experimental data on fixed beds,[25] and the Wen-Yu correlation was based on the homogeneous expansion of fluidized beds.[26] Apparently, the information of the subgrid structures in the Gidaspow model is missing, and therefore, the drag force is overestimated. Theoretically this can be overcome if one uses a grid with a size well below subgrid structure elements,[33−35] but this is certainly not realistic for large scale fluidized bed simulation due to the limitations in the power of the computer.

2.3.2. EMMS Model. A promising approach for drag force calculation is the EMMS model proposed by Li and Kwauk.[37] The EMMS model is based on the multiscale analysis of the momentum and mass conservation in fluidized bed and the hydrodynamic trend toward a compromise between the gas phase and solid phase.[37] It assumes in the EMMS model that the flow consists of a dense cluster phase and a lean surrounding phase. The clusters are assumed to be spherical with the voidage of the clusters equal to the voidage at minimum fluidization velocity. The clusters are assumed homogeneously dispersed in a control volume.[37] The model,

dx.doi.org/10.1021/ie303467k | Ind. Eng. Chem. Res. 2013, 52, 11354−11364

based on these assumptions, can be formulated as a nonlinear optimization problem. The EMMS model was first developed for a CFB riser.[30] It has been found in our simulations that the first version of the EMMS model[30] is not suitable for simulating the hydrodynamics of a fluidized bed for Gledart A particles.

Recently, Shi et al[40] developed an EMMS-bubble model for bubbling gas−solid fluidized beds. In the EMMS-bubble model, the bubbles instead of particle clusters in the fluidized bed are treated as subgrid structures. In this work, the EMMS-bubble model was implemented to account for the influence of the flow heterogeneity on drag force between solids and gases. Following the approach of Shi et al.,[40] the momentum exchange coefficient β is calculated by

$$\beta = \frac{3}{4} C_d \frac{\rho_g (1-\varepsilon)\varepsilon |u-v|}{d_p} \varepsilon^{-2.65} H_d, \text{ for } \varepsilon_g > 0.4 \quad (21)$$

Where H_d can be derived from

$$H_d = \frac{5.8853 - 32.2520\varepsilon_g + 45.8629{\varepsilon_g}^2}{1 - 243.9459\varepsilon_g + 603.6253{\varepsilon_g}^2}, \text{ for } 0.4 \le \varepsilon_g < 0.5 \quad (22a)$$

$$H_d = \frac{0.1496 - 0.4601\varepsilon_g + 0.4833{\varepsilon_g}^2}{1 + 0.0400\varepsilon_g - 0.1777{\varepsilon_g}^2}, \text{ for } 0.5 \le \varepsilon_g < 0.98 \quad (22b)$$

$$H_d = \frac{-1.9894 + 5.7462\varepsilon_g - 3.7486{\varepsilon_g}^2}{1 + 7.0967\varepsilon_g - 8.0508{\varepsilon_g}^2}, \text{ for } 0.98 \le \varepsilon_g < 1 \quad (22c)$$

2.4. MTO Reaction Kinetics. The reaction kinetics for MTO is based on the kinetic model proposed by Najafabadi et al.[45] However, the three coefficients of activation energy given by Najafabadi et al.[45] have been modified in order to fit our mirco-scale fluidized bed experimental data before the simulations. The kinetics study in a microscale fluidized bed reactor will be published elsewhere. The reaction network and some typical parameters are listed in Table 1.

The species transport equation for MTO reactor can be written

$$\frac{\partial(\varepsilon_g \rho_g {m^i}_g)}{\partial t} + \nabla \times (\varepsilon_g \rho_g v_g {m^i}_g) = \nabla \times (\varepsilon_g \rho_g {D^i}_g \nabla {m^i}_g) + {S^i}_{gs} \quad (23)$$

where ${m^i}_g$ is the mass fraction of species i in gas phase, ${D^i}_g$ is the mass diffusion coefficient of the species i, and ${S^i}_{gs}$ is the reaction rate of the species i.

2.5. Coupling between the CFD and Reaction Model. As a first step to build the 3D modeling approach for the DMTO process, a weak coupling between the hydrodynamics and reaction is adopted in order to reduce the computational time. Here, only the influence of the hydrodynamics on reaction kinetics is considered. The CFD simulations are carried out to obtain the detailed flow field parameters such as phase velocities, phase volume fraction, and pressure. These parameters are averaged for a certain period after the fluidization in the fluidized bed is fully developed. The averaged hydrodynamic parameters are then inputted into the species transport equations to calculate the product distribution.

Table 1. Reaction mechanism and the parameters

no.	reaction	pre-exponent, A^b	activation, E (kJ/mol)
1	2MeOH <=> $[(CH_3)_2O] + H_2O$	5.70×10^5	87.1
2[a]	$2[(CH_3)_2O] \rightarrow C_2H_4 +$ 2MeOH	1.70×10^6	76.9
3[a]	$2MeOH \rightarrow C_2H_4 + 2H_2O$	1.90×10^6	112.5
4	$C_2H_4 + DME \rightarrow C_3H_6 +$ MeOH	3.70×10^5	74.0[c]
5	$C_3H_6 + DME \rightarrow C_4H_8 +$ MeOH	2.70×10^6	88.2[c]
6	$C_4H_8 + DME \rightarrow C_5H_{10} +$ MeOH	2.06×10^6	90.4[c]
7	$MeOH \rightarrow CO + 2H_2$	1.60×10^6	113.3
8	$CO + H_2O \rightarrow CO_2 + H_2$	2.00×10^6	119
9	$MeOH + H_2 \rightarrow CH_4 + H_2O$	1.00×10^6	97
10	$C_2H_4 + H_2 \rightarrow C_2H_6$	1.30×10^6	110.3

[a]Reaction is in first order. [b]Unit of A is $m^3/(g\ h)$ in first order and $(m^3)^2/(g\ mol\ h)$ in second order. [c]Value is fitted by our experimental value.

It is argued that if a more accurate and detailed description is required, the influence of the chemical reaction on the continuum equations and momentum equations needs to be taken into account as well. This is because the local gas density and viscosity in the continuum equations and momentum equations will be dynamically changing with time. The mass source term due to the chemical reactions and interphase momentum change source term due to mass transfer should be included in the continuum equations and momentum equations. In this work, however, the two-way coupling between the hydrodynamics and reaction kinetics is not considered. On one hand, the MTO process, depending on the operation conditions, is a volume increasing process. In a commercial unit, the methanol is always fed into the reactor with 20 wt % steam. Note that 56.25 wt % of methanol will be converted directly to H_2O and only 43.75 wt % of methanol will be transferred into low olefins and other byproducts. The volume expansion of the gas inside the reactor, based on a typical product distribution, is less than 15%, which means the gas density change after complete conversion is also less than 15%. Such a relatively small change in the gas density would not have a significant influence on the hydrodynamics. On the other hand, the gas viscosity is more affected by the temperature. In this work, the temperature is considered as the constant, and the change in gas viscosity due to the variation of the compositions can be ignored. We would stressed that, although the one-way coupling between the hydrodynamics and reaction kinetics might cause certain simulation errors, a great saving of computational time can be achieved. The latter is especially important for large scale simulations. In fact, the MTO reaction is a fast reaction, and the time step for reaction kinetics calculation is much smaller than the CFD time step. A two-way coupling between the hydrodynamics and reaction kinetics will lead to an unrealistic computational time.

2.6. Geometry and Mesh. The sketch of the 16 kt/a MTO reactor is shown in Figure 1. The reactor height is 8.5 m. The diameter of the bottom part (stripper) is 0.22 m. The middle part (dense bed) is 1.00 m, and the top part (freeboard) is 1.95 m. In the real setup, the catalyst is flowing into the bed by lift

dx.doi.org/10.1021/ie303467k | Ind. Eng. Chem. Res. 2013, 52, 11354−11364

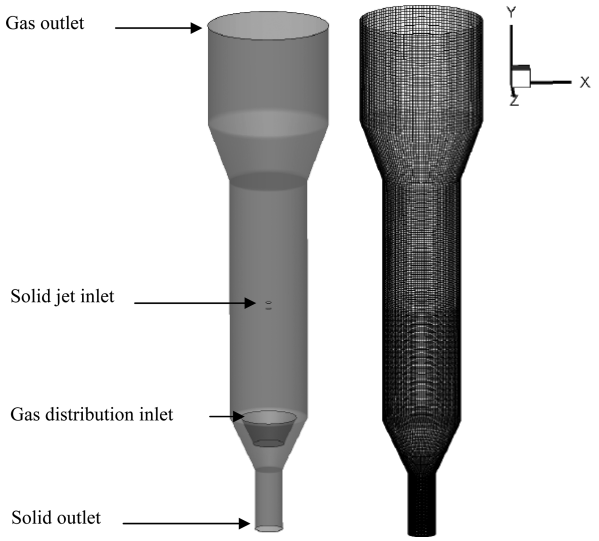

Figure 1. Geometry and surface mesh of the fluidized bed reactor in the 16 kt/a DMTO demonstration unit.

gas through the orifices in a pipe with a length of 0.1 m and diameter of 0.1 m. The gas distributor consists of small nozzles pointing upward, which inject the gas flow at high velocities into the dense bed. However, in our model, the catalyst inlet and gas distributor have been simplified as a cylinder pipe and a circle plate where the catalyst and gas are uniformly flowing into the reactor. This is because the implementation of the fine mesh structure is extremely difficult, if not impossible, with current computational hardware. The catalyst inlet has a length of 0.1 m and diameter of 0.1 m. The flow rate of the catalyst is calculated according to the catalyst circulation rate in the experiments. The velocity of gas from the distributor is calculated based on the gas flow rate. The reactor was divided into several blocks and was meshed with hexahedron. The top part was meshed with a size scale of 0.05 m and the others with size scale of 0.02 m. The origin point is set at the center of the solid outlet surface at the bottom of the reactor, and the *y*-axis is against the gravity direction.

2.7. Simulation Methods. The Eulerian Granular Multiphase Model in Fluent 6.3.26 has been used to simulate the gas−solid two-phase flows. The phase-coupled SIMPLE method was chosen for pressure−velocity coupling, the first-order upwind scheme was used for discretization of momentum and volume fraction equations. The time step size was 0.0005 s. The drag coefficient correction based on the EMMS-bubble model was coupled into Fluent 6.3.26 with user-defined functions (UDF). The species transport equations, eq 23, were solved with the *Gauss upwind* scheme for convection term, *Gauss linear corrected* scheme for diffusion term, and implicit Euler method (first order) for time discretion.

Two sets of different simulations have been carried out. The first set of simulations focused on the study of the drag correlations. In these simulations, only hydrodynamics has been computed, and no reaction is considered. The gas is assumed having a density of 1.20 kg/m^3 and a viscosity of 1.8×10^{-5} Pa s. The second set of simulations mainly dealt with the reaction kinetics. In this set of simulations, the hydrodynamics was first calculated by the two-fluid model, where the gas density and viscosity were set as 0.37 kg/m^3 and 2.4×10^{-5} Pa s, respectively. The hydrodynamic parameters were averaged for a certain period after the fluidization fully developed. The averaged hydrodynamic parameters were then fed into the species transport equations to calculate the product distribution. Some of the simulation conditions are listed in Table 2.

Table 2. Simulation Conditions

	values	
properties	case 1: without reaction	case 2: with reaction
particle density (kg/m^3)	1500	
particle diameter (m)	7.5×10^{-5}	
gas density	1.2 kg/m^3	0.37 kg/m^3
gas viscosity	1.8×10^{-5} Pa.s	2.4×10^{-5} Pa.s
bed temperature	293 K	723 K
initial bed height	3 m	
boundary Conditions		
gas inlet	constant gas velocity, 1.86 m/s	
gas outlet	gas pressure, 101325 Pa	
catalyst circulation rate	400 kg/h	
wall	no-slip for both phase	

3. RESULTS AND DISCUSSION

3.1. Drag Model. The MTO reactor studied in this research is essentially operating in the turbulent bed regime, and the catalyst used is belonging to the Geldart A type of particles. In the turbulent fluidized bed regime, the mass transfer between the gas phase and solid phase will be enhanced. Both the Gidaspow and EMMS-bubbling drag model have been tested. In the simulations, the bed temperature is set to 293 K, and no reaction is turned on. For comparison, we plot the simulation results for both the Gidaspow and EMMS-bubbling drag force model in Figure 2. As shown, no stable dense bed has been found in the simulation based on the Gidaspow drag model, and an unrealistically high bed expansion is observed. Meanwhile the EMMS-bubbling model could predict the solid fraction distribution reasonable well. We have compared the axial profiles of the average solid volume fraction ε_s (averaged over the cross section) obtained from the simulations with the experimental data, as shown in Figure 3. The experimental results were obtained from the operating data of the 16kt/a DMTO demonstration unit. As shown, the solid fraction, ε_s, has an apparent gradient from the bottom to the top. The simulation results based on the Gidaspow model clearly underestimated the solid fraction in the stripper part. This is also shown in Figure 4. The solid fraction predicted by the Gidaspow model is less than 0.2, which is in the range of the riser reactor. The axial profile of the simulation results based on the EMMS-bubbling model, however, agree generally well with the experimental data.

3.2. Gas−Solid Distribution. The efficiency of the reactor depends strongly on the solid−gas distribution because the catalytic reaction mostly takes place in the emulsion phase. From Figure 4, it can be demonstrated that the solid volume fraction is lower in the center and higher near the wall, which reveals a core−annulus structure. Such a core−annulus structure may be related to the gas distributor configuration. As shown in Figure 1, our gas distributor is installed in the center of the bed, and the spent catalyst leaves the reactor from the annulus zone to the stripper. By this gas distributor configuration, most of gas enters the reactor from the center

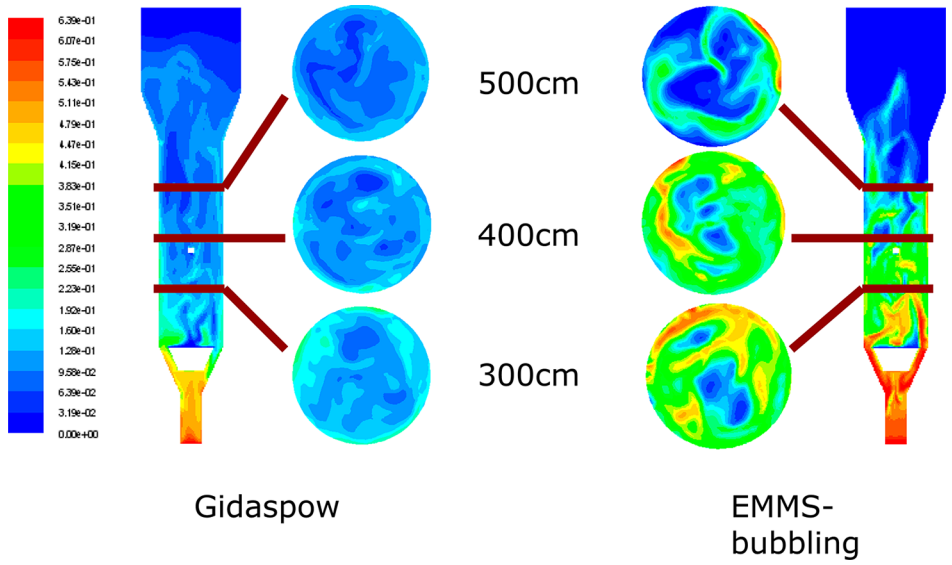

Figure 2. Simulated solid fraction distribution in the reactor: 2D sectional view of the $X-Y$ plane. Simulations results based on (left) Gidaspow model and (right) EMMS-bubbling model with a bed temperature of 293 K, gas density of 1.2 kg/m^3, and gas viscosity of 1.8×10^{-5} Pa s. Other simulation conditions are specified in Table 2.

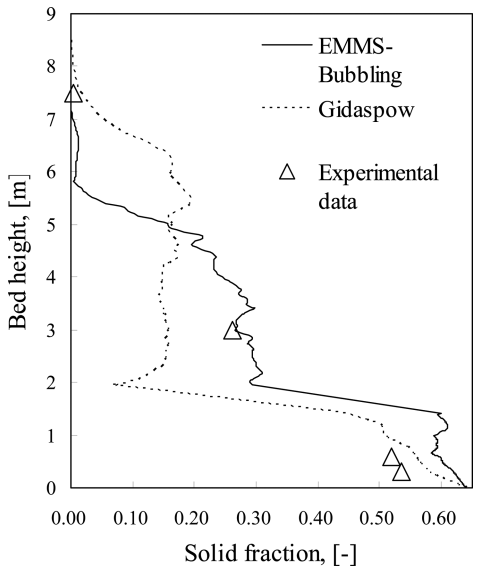

Figure 3. Axial profiles of the cross-sectionally averaged solid volume fraction obtained from the simulation results based on the Gidapow drag force model, EMMS-bubble drag force model, and experimental data. Simulation conditions are the same as in Figure 2.

zone and leads to a relatively dilute zone of catalyst in the middle of the fluidized bed.

Close checking of the results from the EMMS-bubbling model discovers that the bed is actually chaotic, and there is no clear up surface at the top of the dense bed. The entrainment of catalyst is high, and hence, a large amount of catalyst is carried to the freeboard. These are typical phenomenon in turbulent fluidized bed reactors. In the bottom (stripper) section, the catalyst flows down along the axis of the reactor by gravity. Thus, the catalyst in the stripper section is in fact in a very dense bubbling bed regime. The gas is dragged down by the catalyst in this regime.

3.3. Solid and Gas Phase Velocity. Figure 5a shows the simulated distribution of solid velocity in the y-direction (counter-gravity) at different bed height. It shows that the solid velocity in the y-direction is mainly positive in the center and negative near the wall. This further confirms the core−annulus structure. By comparison of these slices, it has been found that severe fluctuation happens at the top of the bed. At the middle of the dense bed (300 cm height), the solid phase velocity has a relatively narrow distribution, as shown in Figure 5b, and particles in the region near the wall have high downward velocity. A comparison of the results based on the EMMS-

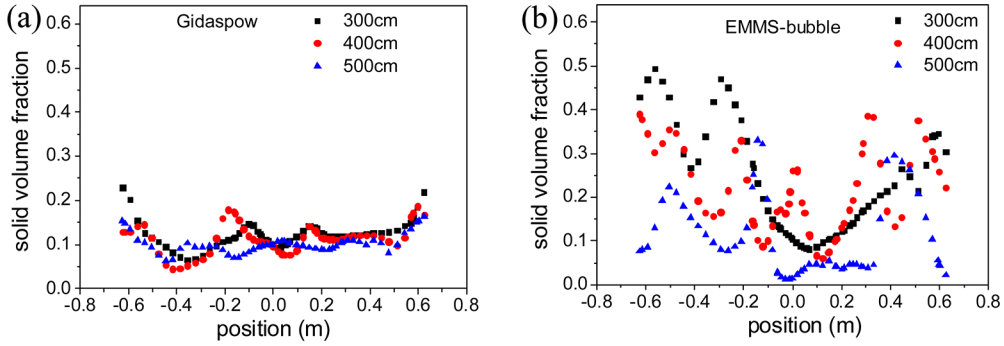

Figure 4. Cross-sectional solid volume fraction distribution at different height of the fluidized bed reactor in the 16kt/a DMTO demonstration unit. Results are obtained from the simulations, with the same simulation conditions as in Figure 2.

dx.doi.org/10.1021/ie303467k | Ind. Eng. Chem. Res. 2013, 52, 11354−11364

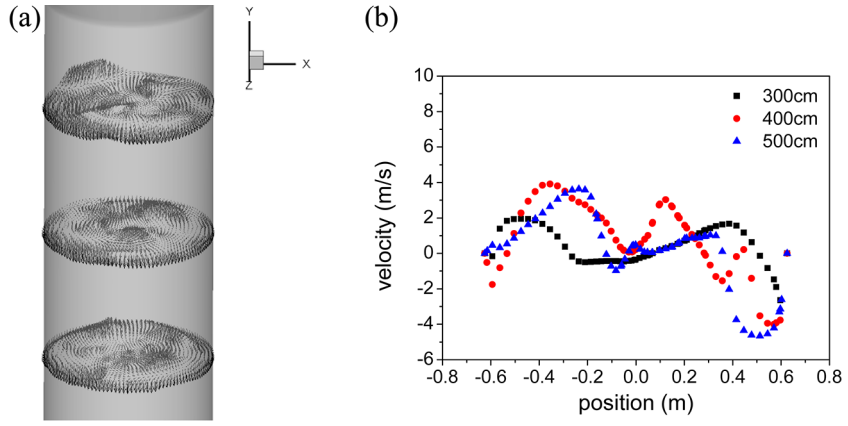

Figure 5. Axial solid velocity at different heights of the fluidized bed reactor in the 16kt/a DMTO demonstration unit. Results are obtained from the simulations with the EMMS-bubbling drag force model, and the other simulation conditions are the same as in Figure 2.

bubbling model and Gidaspow model is also plotted in Figure 6. As shown, the Gidaspow model generally predicted a higher axial solid velocity.

Figures 7 and 8 show the axial gas velocity distribution. The results show that the velocities of the particle and gas phase have similar distribution.

3.4. Results of MTO Reactions. On the basis of the hydrodynamics predicted by the TFM coupled with the EMMS-bubbling model, a preliminary study on the MTO reaction in the 16 kt/a fluidized bed reactor has been carried out, and the results are compared with the experimental data. In the TFM simulations, the bed temperature is set to 723 K, and the reaction is turned on. The hydrodynamics data is averaged over a certain period when the fluidized bed reactor is fully fluidized after sufficiently long time simulations. In Figure 9, the instantaneous solid fraction distribution, after the gas−solid flow has been fully developed, is shown.

The simulation results of the selectivity of the main gas components are plotted in Figure 10, where the experimental data is included for comparison. It can be seen from the results that the predicted selectivity of ethylene and propylene is lower than the experimental data, while the predicted CO_2 is much higher that the experimental data. In Figure 11, the 3D distribution of the methanol concentration is shown. Clearly, the methanol is converted rapidly in the reactor. Only near the gas distributor some methanol can be detected, which is in lines with our observation in the experiments. At the gas outlet, the methanol concentration is almost zero, which means it has been completely converted in the bed. In Figure 12, the concentration distributions of C_2H_4, C_3H_6, and H_2O are shown. As can be seen, for C_3H_6 and H_2O, the concentration is quite homogeneous in the bed except in the regime near the gas inlet. However, the C_2H_4 shows a distribution in the dense bed. Qualitatively, the simulation results of the 16 kt/a DMTO fluidized bed reactor are in accordance with the experimental observation.

The deviation of the selectivity may be due to two reasons. First, the catalyst used when developing the kinetics is certainly different from the commercial DMTO catalyst. Different catalysts lead to different kinetic parameters. Second, the MTO reaction network by Najafabadi et al.[45] does not take the coke formation kinetics into account. It has been widely accepted that the catalyst with a certain amount of coke favors the selectivity of the ethylene and propylene in MTO reactions. Excluding the coke formation kinetics may cause the predicted low olefins selectivity to deviate from the experimental data. A detailed MTO kinetics model, including the coke formation kinetics, is being developed now.

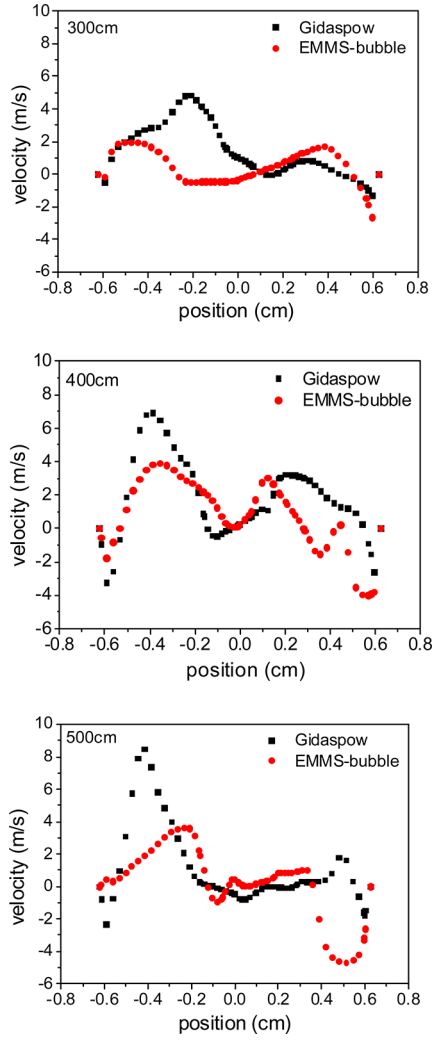

Figure 6. Axial solid velocity at different height of the fluidized bed reactor in the 16kt/a DMTO demonstration unit. Results are obtained from the simulations with either the Gidaspow drag force model or EMMS-bubbling drag force model, and the other simulation conditions are the same as in Figure 2.

dx.doi.org/10.1021/ie303467k | *Ind. Eng. Chem. Res.* 2013, 52, 11354−11364

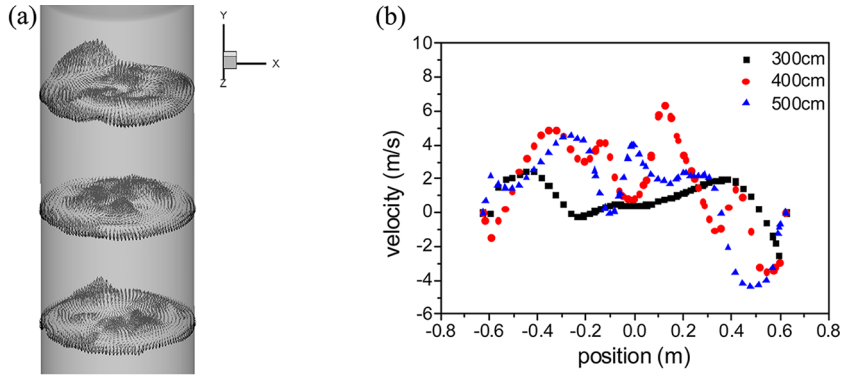

Figure 7. Axial gas velocity at different height of the fluidized bed reactor in the 16kt/a DMTO demonstration unit. Results are obtained from the simulations with the EMMS-bubbling drag force model, and the other simulation conditions are the same as in Figure 2.

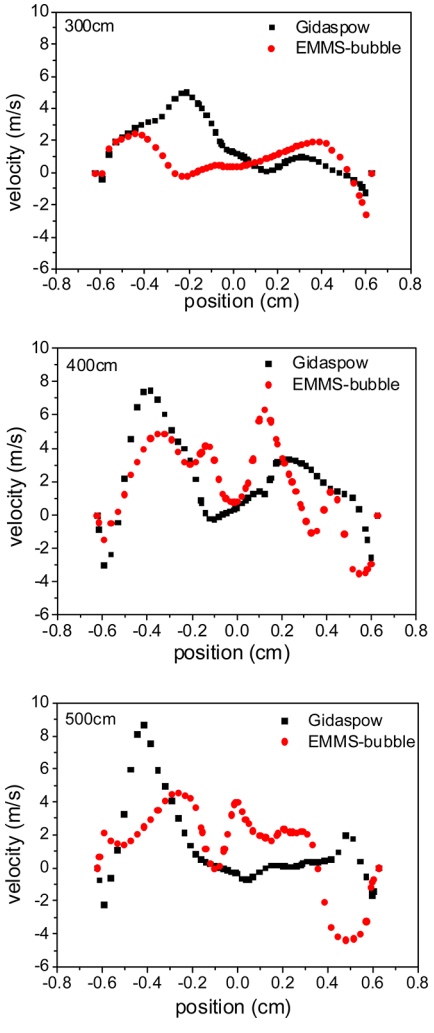

Figure 8. Axial gas velocity at different height of the fluidized bed reactor in the 16kt/a DMTO demonstration unit. Results are obtained from the simulations with either the Gidaspow drag force model or EMMS-bubbling drag force model, and the other simulation conditions are the same as in Figure 2.

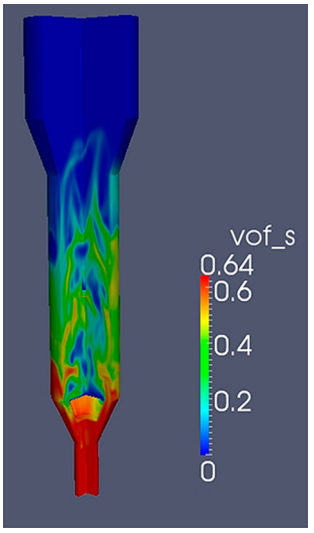

Figure 9. Simulated solid fraction distribution in the 16 kt/a DMTO fluidized bed reactor: 3D view. Simulation results based on the EMMS-bubbling model, with a bed temperature of 723 K, gas density of 0.37 kg/m^3, and gas viscosity of 2.4 × 10^{-5} Pa s. Other simulation conditions are specified in Table 2.

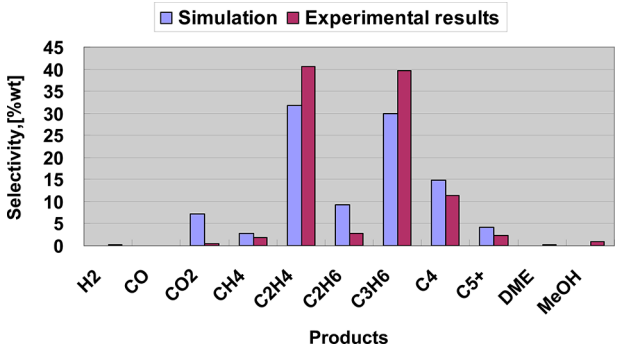

Figure 10. Experimental and simulation results of products (dry gas) selectivity at the outlet of 16 kt/a DMTO fluidized bed reactor. Simulation results based on the EMMS-bubbling model, with a bed temperature of 723 K, gas density of 0.37 kg/m^3, and gas viscosity of 2.4 × 10^{-5} Pa s. Other simulation conditions are specified in Table 2.

It is also interesting to note that the MTO reaction mostly takes place in the regime near the gas distributor. Actually, the methanol conversion could be completed in the time scale of 10^{-3} second. Therefore the solid−gas two-phase flows near the gas distributor should be most important in the MTO reactor, which determines the methanol transformation into light olefins. A more detailed study of the flow structure near the gas distributor is highly required. The solid−gas two-phase flow patterns in the rest of the bed is also critical because it may lead

dx.doi.org/10.1021/ie303467k | Ind. Eng. Chem. Res. 2013, 52, 11354−11364

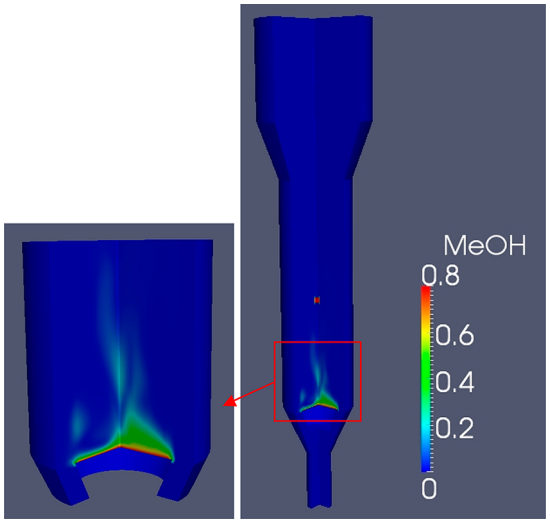

Figure 11. Concentration distribution of MeOH inside the 16 kt/a DMTO fluidized bed reactor. Simulations conditions are the same as in Figure 10.

to further conversion of the light olefins and C_4+ into undesired product.

4. CONCLUSION

In this paper, we report on our preliminary work on establishing a 3D modeling approach for the 16 kt/a DMTO fluidized bed reactor. The two-fluid model (TFM) has been used, in which the kinetic theory of granular flows was used as the closure correlations for particle phase pressure and particle phase viscosity. As the gas−solid interaction dominates the subgrid flow structure in the fluidized bed, the EMMS-bubbling model, in which the subgrid bubble behavior is taken into account, was chosen to calculate the drag forces between solids and gas. Simulation results show that the traditional Gidaspow model cannot predict a stable dense bed, while the EMMS-bubbling mode could predict the solid fraction distribution reasonably well. A core−annulus structure was observed in the simulations, which may be related to the gas distributor configuration where the gas enters the center of the bed from the center and the spent catalyst leaves the reactor from the annulus zone. A simple reaction model was implemented to study the MTO reaction in the 16 kt/a fluidized bed reactor. It has been found that the selectivity of ethylene and propylene are lower than the experimental data, but the selectivity of CO_2 is higher. The methanol is converted rapidly in the reactor, and only near the gas distributor some unconverted methanol is detected. These results are in accordance with our qualitative observation.

It should be stressed that the work reported in this paper is just the first step. The TFM, if coupled with the EMMS-bubbling model, can be used to investigate the hydrodynamics in the large scale fluidized bed reactor. Some important features of the 16 kt/a MTO fluidized bed reactor can be demonstrated in the simulations, but it should also be noted that the MTO fluidized bed was operating in the turbulent fluidization regime. The EMMS-bubbling model was originally developed for the bubbling fluidized beds. A further extension of the EMMS model to turbulent fluidized bed is desired in order to get more quantitative results.

The MTO reaction kinetics used in this paper is not specifically for a DMTO commercial catalyst. Moreover, the reaction kinetics implemented in the current work does not take the effect of the coke-in-catalyst into account. It has been widely accepted that the catalyst deposited with a certain amount of coke favors the selectivity of the ethylene and propylene in MTO reactions. It is therefore not surprising that the simulated results of the selectivity show some deviation from the experimental data. Establishing a reliable MTO reaction kinetics for a DMTO commercial catalyst is undergoing.

AUTHOR INFORMATION

Corresponding Author

*E-mail: maoye@dicp.ac.cn.

Notes

The authors declare no competing financial interest.

ACKNOWLEDGMENTS

The authors appreciate Professor Jinghai Li and his group at the Institute of Process Engineering, Chinese Academy of Sciences

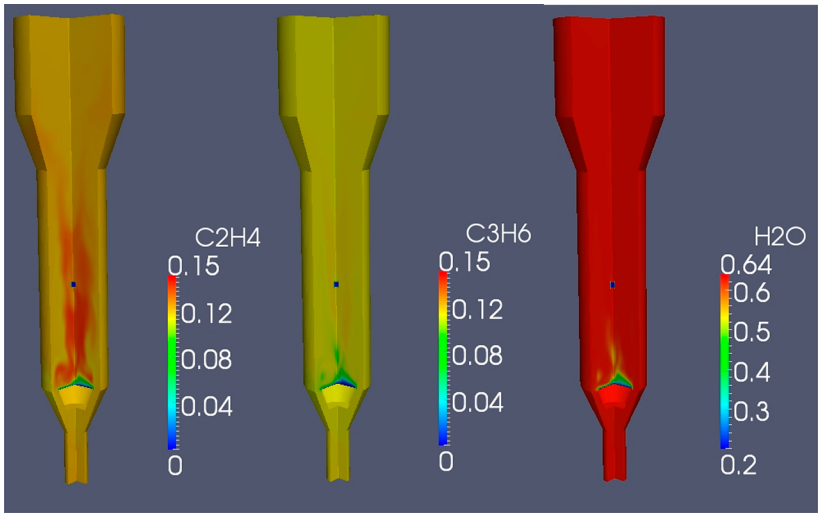

Figure 12. Concentration distribution of C_2H_4, C_3H_6, and H_2O inside the 16 kt/a DMTO fluidized bed reactor. Simulations conditions are the same as in Figure 10.

for sharing the EMMS-bubbling model source code and providing technical support in this work. This work is supported by the Knowledge Innovation Program of the Chinese Academy of Sciences (Project "Study of fluidization in methanol to olefins (MTO) process"), Strategic Priority Research Program of the Chinese Academy of Sciences (Grant XDA07080302), and National High-tech R&D Program of China (863 Program) (Grant 2012AA051001).

NOTATION

C_d = drag coefficient
d_s = particle diameter (m)
e = coefficient of restitution for particle collisions
g = gravitational accelerarion (m/s^2)
g_0 = radial distribution function, dimensionless
G_s = solid flux (kg/(m^{2}s))
H_d = heterogeneity index of the drag coefficient correction
p = pressure (Pa)
Re = Reynolds number
Ug, Us (m/s) = superficial velocity of gas and particle
v_g, v_s (m/s) = local velocity of gas and particle

Greek Letters

ε volume fraction
μ shear viscosity (Pa s)
ρ density (kg/m^3)
β interphase momentum exchange cofficient (kg/(m^{3}s))
Θ guanular temperature (m^2/s^2)
κ_Θ diffusion coefficient of energy (kg/(m s))
λ bulk viscosity (Pa s)
τ stress−strain tensor (Pa)
Φ angle of internal friction (deg)

Subscripts

g gas phase
s solid phase

REFERENCES

(1) Chang, C. D. Hydrocarbons from methanol. *Catal. Rev.* **1983**, *25*, 1−118.
(2) Liu, Z.; Liang, J. Methanol to olefin conversion catalysts. *Curr. Opin. Solid State Mater. Sci.* **1999**, *4*, 80−84.
(3) Keil, F. J. Methanol-to-hydrocarbons: Process technology. *Microporous Mesoporous Mater.* **1999**, *29*, 49−66.
(4) Liang, J.; Li, H.; Zhao, S.; Guo, W.; Wang, R.; Yang, M. Characteristics and performance of SAPO-34 catalyst for methanol-to-olefin conversion. *Appl. Catal.* **1990**, *64*, 31−40.
(5) Dahl, I. M.; Kolboe, S. On the reaction-mechanism for propene formation in the MTO reaction over SAPO-34. *Catal. Lett.* **1993**, *20*, 329−336.
(6) Haw, J. F.; Song, W.; Marcus, D. M.; Nicholas, J. B. The mechanism of methanol to hydrocarbon catalysis. *Acc. Chem. Res.* **2003**, *36*, 317−326.
(7) Bos, A. N. R.; Tromp, P. J. J.; Akse, H. N. Conversion of methanol to lower olefins: Kinetic modeling, reactor simulation, and selection. *Ind. Eng. Chem. Res.* **1995**, *34*, 3808−3816.
(8) Alwahabi, S. M.; Froment, G. F. Single event kinetic modeling of the methanol-to-olefins process on SAPO-34. *Ind. Eng. Chem. Res.* **2004**, *43*, 5098−5111.
(9) Chen, D.; Rebo, H. P.; Moljord, K.; Holmen, A. Methanol conversion to light olefins over SAPO-34. Sorption, diffusion, and catalytic reactions. *Ind. Eng. Chem. Res.* **1999**, *38*, 4241−4249.
(10) Soundararajan, S.; Dalai, A. K.; Berruti, F. Modeling of methanol to olefins (MTO) process in a circulating fluidized bed reactor. *Fuel.* **2001**, *80*, 1187−1197.
(11) Tsuji, Y.; Kawaguchi, T.; Tanaka, T. Discrete particle simulation of 2-dimensional fluidized-bed. *Powder Technol.* **1993**, *77*, 79−87.
(12) Hoomans, B. P. B.; Kuipers, J. A. M.; Briels, W. J.; van Swaaij, W. P. M. Discrete particle simulation of bubble and slug formation in a two-dimensional gas-fluidised bed: A hard-sphere approach. *Chem. Eng. Sci.* **1996**, *51*, 99−118.
(13) Xu, B. H.; Yu, A. B. Numerical simulation of the gas-solid flow in a fluidized bed by combining discrete particle method with computational fluid dynamics. *Chem. Eng. Sci.* **1997**, *52*, 2786−2809.
(14) Ouyang, J.; Li, J. Particle-motion-resolved discrete model for simulating gas-solid fluidization. *Chem. Eng. Sci.* **1999**, *54*, 2077−2083.
(15) Ye, M.; Van der Hoef, M. A.; Kuipers, J. A. M. A numerical study of fluidization behavior of Geldart A particles using a discrete particle model. *Powder Technol.* **2004**, *139*, 129−139.
(16) Ding, J.; Gidaspow, D. A bubbling fluidization model using kinetic theory of granular flow. *AIChE J.* **1990**, *36*, 523−538.
(17) Kuipers, J. A. M.; Van Duin, K. J.; Van Beckum, F. P. H.; Van Swaaij, W. P. M. A numerical model of gas-fluidized beds. *Chem. Eng. Sci.* **1992**, *47*, 1913−1924.
(18) Enwald, H.; Peirano, E.; Almstedt, A. E. Eulerian two-phase flow theory applied to fluidization. *Int. J. Multiphase Flow* **1996**, *22*, 21−66.
(19) van Wachem, B. G. M.; Schouten, J. C.; Krishna, R.; van den Bleek, C. M.; Sinclair, J. L. Comparative analysis of CFD models of dense gas-solid systems. *AIChE J.* **2001**, *47*, 1035−1051.
(20) Yang, N.; Wang, W.; Ge, W.; Wang, L.; Li, J. Simulation of heterogeneous structure in a circulating fluidized-bed riser by combining the two-fluid model with the EMMS approach. *Ind. Eng. Chem. Res.* **2004**, *43*, 5548−5561.
(21) Wang, J. A review of Eulerian simulation of Geldart A particles in gas-fluidized beds. *Ind. Eng. Chem. Res.* **2009**, *48*, 5567−5577.
(22) Gidaspow, D. Multiphase Flow and Fluidization: Continuum and Kinetic Theory Description; Academic Press: Boston, 1994.
(23) Gibilaro, L. G.; Di Felice, R.; Waldram, S. P.; Foscolo, P. U. Generalized friction factor and drag coefficient correlations for fluid-particle interactions. *Chem. Eng. Sci.* **1985**, *40*, 1817−1823.
(24) Huilin, L.; He, Y.; Gidaspow, D. Hydrodynamic modelling of binary mixture in a gas bubbling fluidized bed using the kinetic theory of granular flow. *Chem. Eng. Sci.* **2003**, *58*, 1197−1205.
(25) Ergun, S. Fluid flow through packed columns. *Chem. Eng. Prog.* **1952**, *48*, 89−95.
(26) Wen, C. Y.; Yu, Y. H. Mechanics of fluidization. *Chem. Eng. Prog. Symp.* **1966**, *62*, 100−111.
(27) O'Brien, T. J.; Syamlal, M. Particle Cluster Effects in the Numerical Simulation of a Circulating Fluidized Bed. In *Circulating Fluidized Bed Technology IV*; Avidan, A. A., Ed.; Mobil Research and Development Corporation: Maricopa, AZ; 1993; 345−350.
(28) Hill, R. J.; Koch, D. L.; Ladd, J. C. The first effects of fluid inertia on flows in ordered and random arrays of spheres. *J. Fluid Mech.* **2001**, *448*, 213−241.
(29) Beetstra, R.; van der Hoef, M. A.; Kuipers, J. A. M. Numerical study of segregation using a new drag force correlation for polydisperse systems derived from lattice-Boltzmann simulations. *Chem. Eng. Sci.* **2007**, *62*, 246−255.
(30) Yang, N.; Wang, W.; Ge, W.; Li, J. Choosing structure-dependent drag coefficient in modeling gas−solid two-phase flow. *Chin. Particuol.* **2003**, *1*, 38−41.
(31) Ye, M.; Wang, J.; Van der Hoef, M. A.; Kuipers, J. A. M. Two fluid modeling of Geldart A particles in gas-fluidized beds. *Particuology* **2008**, *6*, 540−548.
(32) Mckeen, T.; Pugsley, T. Simulation and experimental validation of a freely bubbling bed of FCC catalyst. *Powder Technol.* **2003**, *129*, 139−152.
(33) Wang, J.; Van der Hoef, M. A.; Kuipers, J. A. M. The role of scale resolution versus inter-particle cohesive forces in two-fluid modeling of bubbling fluidization of Geldart A particles. *Chem. Eng. Sci.* **2011**, *66*, 4229−4240.
(34) Wang, J.; Van der Hoef, M. A.; Kuipers, J. A. M. CFD study of the minimum bubbling velocity of Geldart A particles in gas-fluidized beds. *Chem. Eng. Sci.* **2010**, *65*, 3772−3785.
(35) Wang, J.; Van der Hoef, M. A.; Kuipers, J. A. M. Why the two-fluid model fails to predict the bed expansion characteristics of Geldart

A particles in gas-fluidized beds: A tentative answer. *Chem. Eng. Sci.* **2009**, *64*, 622−625.
(36) Andrews, A. T. I.; Loezos, P. N.; Sundaresan, S. Coarse-grid simulation of gas-particle flows in vertical risers. *Ind. Eng. Chem. Res.* **2005**, *44*, 6022−6037.
(37) Li, J.; Kwauk, M. Particle-Fluid Two-Phase Flow: The Energy Minimization Multi-Scale Method; Metallurgical Industry Press: Beijing, P.R. China, 1994.
(38) Wang, W.; Li, J. Simulation of gas−solid two-phase flow by a multi-scale CFD approach-Extension of the EMMS model to the sub-grid level. *Chem. Eng. Sci.* **2007**, *62*, 208−231.
(39) Yang, N.; Wang, W.; Ge, W.; Li, J. CFD simulation of concurrent-up gas−solid flow in circulating fluidized beds with structure-dependent drag coefficient. *Chem. Eng. J.* **2003**, *96*, 71−80.
(40) Shi, Z.; Wang, W.; Li, J. A bubble-based EMMS model for gas−solid bubbling fluidization. *Chem. Eng. Sci.* **2011**, *66*, 5541−5555.
(41) Lu, B.; Wang, W.; Li, J.; Wang, X.; Gao, S.; Lu, W.; Xu, Y.; Long, J. Multi-scale CFD simulation of gas−solid flow in MIP reactors with a structure-dependent drag model. *Chem. Eng. Sci.* **2007**, *62*, 5487−5494.
(42) Nikolopoulos, A.; Papafotiou, D.; Nikolopoulos, N.; Grammelis, P.; Kakaras, E. An advanced EMMS scheme for the prediction of drag coefficient under a 1.2MWth CFBC isothermal flow – Part I: Numerical formulation. *Chem. Eng. Sci.* **2010**, *65*, 4080−4088.
(43) Nikolopoulos, A.; Atsonios, K.; Nikolopoulos, N.; Grammelis, P.; Kakaras, E. An advanced EMMS scheme for the prediction of drag coefficient under a 1.2MWth CFBC isothermal flow – Part II: Numerical implementation. *Chem. Eng. Sci.* **2010**, *65*, 4089−4099.
(44) Lun, C. K. K.; Savage, S. B.; Jeffrey, D. J.; Chepurniy, N. Kinetic theories for granular flow: Inelastic particles in couette flow and slightly inelastic particles in a general flow field. *J. Fluid Mech.* **1984**, *140*, 223−256.
(45) Najafabadi, A. T.; Fatemi, S.; Sohrabi, M.; Salmasi, M. Kinetic modeling and optimization of the operating condition of MTO process on SAPO-34 catalyst. *J. Ind. Eng. Chem.* **2012**, *18*, 29−29.
(46) Syamlal, M.; Rogers, W.; O'Brien, T. J. *MFIX Documentation Theory Guide;* ; Technical Report DOE/METC-94/1004; U.S. Department of Energy (DOE), Morgantown Energy Technology Center: Morgantown, WV, 1993.